# Useful QCM Info

#### Kenneth R. Shull et al.

#### Contents

1	Theory	1
2	Extension to 2 Layers 2.1 Special Case - Film Immersed in Liquid	<b>3</b> 4
3	Thin Films3.1 Single Layer3.2 Two Layers3.2.1 Obtaining $J''$ from the dissipation3.2.2 Perfectly Rigid Membrane3.2.3 Obtaining $J^*$ or $G^*$	4 5 5 5 5
4	Solution Method and Error Analysis	6
5	Some Other Expressions 5.1 Voigt Model	<b>6</b> 7
6	Error determination for $J_3''$	8
Bi	ibliography	8

# 1 Theory

As the name implies, the quartz crystal microbalance (QCM) is most often employed as a high sensitivity massbalance. The instrument relies on the piezoelectric nature of quartz to measure changes in resonance frequency caused by the application of a material to the quartz surface. An adsorbed mass or deposited film results in a decrease in resonant frequency of the quartz crystal by an amount,  $\Delta f_{sn}$ , that is given by the well-known Sauerbrey expression[1]:

$$\Delta f_{sn} = \frac{2nf_1^2}{Z_q} \Delta M_A = \frac{2nf_1^2}{Z_q} \rho_f d_f \tag{1}$$

Here, n is the order of the resonance harmonic,  $f_1$  is the fundamental resonance frequency of quartz (5 MHz),  $Z_q$  is its acoustic shear impedance (8.84 × 10<sup>6</sup> kg/m<sup>2</sup>s for AT cut quartz),  $\Delta M_A$  is the mass per unit area of the film,  $\rho$  is its density and d is its thickness. Note that  $\rho d$  is the mass per unit area.

Originally, the technique was designed for use in an air or vacuum environment, but today the QCM is often used to characterize molecules, particles and thin-films in liquid media. Applications include studies of adsorption[2–10], self-assembly[2–4], cell-substrate interactions[11], and electrochemistry[12, 13].

The QCM consists of a single-crystal quartz disc sandwiched between two electrodes. Due to the piezoelectric nature of quartz, the material will oscillate transversely if an alternating potential is applied across the electrodes, propagating a shear wave through the disc. If the frequency of oscillation is near to the acoustic resonance frequency of quartz, a standing shear wave will generate across the disc, inducing a peak in the system conductance.[14, 15] For the AT-cut crystals used throughout this work, the fundamental resonant frequency is

near 5 MHz. The conductance also peaks at odd harmonics (n) of the fundamental resonant frequency, with resonances at 15 MHz (n=3), 25 MHz (n=5), etc. If the conductance is plotted in the frequency domain, Lorentzian curves can be fit to the conductance peaks to provide two values: the resonance frequency ( $f_n$ ), where the conductance is maximum at the n<sup>th</sup> harmonic, and the half-bandwidth ( $\Gamma_n$ ), the half-width at half-maximum of the conductance peak. This half-bandwidth is equal to  $2D/f_n$ , where D is the dissipation factor introduced by the Chalmers group and utilized in the commonly employed time-domain QCM-D technique[16]. We refer to  $\Gamma_n$  simply as the dissipation, recognizing that our definition of the dissipation differs from the QCM-D definition by a factor of  $2/f_n$ .

If a load is applied to the QCM surface,  $f_n$  and  $\Gamma_n$  shift relative to the bare crystal and together make up a complex frequency shift[14, 15]:

$$\Delta f_n^* = \Delta f_n + i \Delta \Gamma_n \tag{2}$$

Note that in our notation, starred quantities are complex, and quantities subscripted with an n depend on the harmonic at which they are measured. When the frequency shift is small in comparison to the resonance frequency of quartz, which is true in nearly all applications of the QCM,  $\Delta f_n^*$  is related to the shift in complex load impedance  $(\Delta Z_{nL}^*)$  through the small load approximation[14]:

$$\Delta f_n^* = \frac{i f_1 \Delta Z_{nL}^*}{\pi Z_q} \tag{3}$$

The Sauerbrey equation can be obtained by substituting from Eq. 3 by using the following inertial load impedance,  $\Delta Z_{ns}^*$  for  $\Delta Z_{nl}^*$ :

$$\Delta Z_{sn}^* = 2\pi i n f_1 \rho_f d_f \tag{4}$$

If the load applied to the quartz surface is a sufficiently thin and rigid film, the half-bandwidth shift goes to zero and the frequency shift reduces to the Sauerbrey expression (eq 1)[1]. For thicker films, the complex resonant frequency deviates from the Sauerbrey relationship and depends on the rheological properties of the material in contact with the crystal surface. To understand the analysis that is used to quantitatively extract these rheological properties from the measured frequency response, it is useful to review some fundamental expressions related to the propagation of shear waves in viscoelastic materials, and to introduce the notation that we use in our work. The acoustic impedance of a bulk material is related to its density and complex shear modulus,  $G_n^*$ :

$$Z_n^* = (\rho G_n^*)^{1/2} \tag{5}$$

Here we choose to express  $G_n^*$  in terms of its magnitude and phase angle:

$$G_n^* = |G_n^*| \exp(i\phi_n) \tag{6}$$

The complex wave vector,  $k_n^*$ , for shear wave propagation in the material can be obtained directly from  $Z_n^*$ [17]:

$$k_n^* = \frac{2\pi f_n \rho}{Z_n^*} \tag{7}$$

The wavelength of the propagating shear wave is then obtained from the real part of  $k^*$  [17]:

$$\lambda_n = \frac{2\pi}{\text{Re}(k_n^*)} = \frac{1}{f_n} \left(\frac{|G_n^*|}{\rho}\right)^{1/2} \frac{1}{\cos(\phi_n/2)}$$
(8)

Finally, we define a quantity,  $D_n^*$ , which plays an important role in the expressions given below:

$$D_n^* = k_n^* d = \frac{2\pi d}{\lambda_n} \left( 1 - i \tan \left( \frac{\phi_n}{2} \right) \right) = \frac{2\pi f_n d\rho}{Z_n^*}$$
 (9)

The properties appearing in Eqs. 5-9 are properties of a single, homogeneous material. We can also write  $Z_n^*$  in terms of  $D_n^*$ :

$$Z_n^* = \frac{2\pi f_n d\rho}{D_n^*} \tag{10}$$

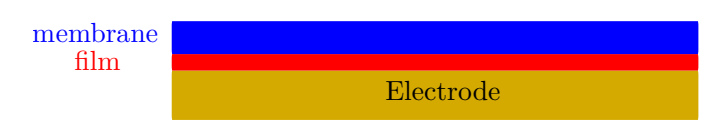


Figure 1: Two-layer geometry involving a 'film' that is sandwiched between the electrode surface and a 'membrane'.

## 2 Extension to 2 Layers

In a variety of situations we are interested in two layer geometries, where the film we are interested in is sand-wiched between the electrode surface of the QCM and a second layer, which we refer to the membrane layer. In our notation the acoustic shear impedance of the membrane layer at the nth harmonic is  $Z_{nm}^*$ ,  $k_{nm}^*$  is the corresponding wave vector and  $d_m$  is the membrane thickness. The overall impedance of this two-layer system is (Eq. 18 from Johannsmann's 1999 paper) [18]:

$$Z_{nfm}^* = Z_{nf}^* \frac{iZ_{nf}^* \tan(k_{nf}^* d_f) + iZ_{nm}^* \tan(k_{nm}^* d_m))}{Z_{nf}^* - Z_{nm}^* \tan(k_{nm}^* d) \tan(k_{nf}^* d)}$$
(11)

We can write this in a more useful way by writing the membrane impedance, in the following way (following our previous notation) [19, 20]:

$$Z_{nm,0}^* = iZ_{nm}^* \tan(k_{nm}^* d_m) \tag{12}$$

The difference between the 2-layer impedance and the impedance of the membrane layer itself is defined as:

$$\Delta Z_{nfm}^* \equiv Z_{nf}^* \frac{i Z_{nf}^* \tan(k_{nf}^* d) + Z_{nm,0}^*}{Z_{nf}^* + i Z_{nm,0}^* \tan(k_{nf}^* d)} - Z_{nm,0}^*$$
(13)

We can apply Eq. 3, with  $\Delta Z_{nL}^* = \Delta Z_{nfm}^*$  to get an expression for the complex frequency shift. After a bunch of algebra, we get to the following form of the master equation:

$$\frac{\Delta f_n^*}{f_{sn}} = -\frac{\tan(D_{nf}^*)}{D_{nf}^*} \left[ \frac{1 - \left(r_{nfm}^*\right)^2}{1 + ir_{nfm}^* \tan(D_{nf}^*)} \right]$$
(14)

Where  $r^*$  is the ratio of the overall membrane impedance to the material impedance for the film:

$$r_{nfm}^* = \frac{Z_{nm,0}^*}{Z_{nf}^*} = D_{nf}^* \frac{Z_{nm,0}^*}{2\pi f_n d\rho}$$
 (15)

Written in this way it's a bit more obvious that there is no net response for the trivial case when a thin film and thick membrane have identical properties ( $r_{nfm}^* = 1$ ), and that the single layer master equation is recovered for experiments done in air ( $r_{nfm}^* = 0$ ).

Note that we define  $\Delta f_{sn}$  as a positive number (see Eq. 1), so in the case where the Sauerbrey limit applies  $(d/\lambda_n \ll 1)$ , and when there is sufficient acoustic contrast between the film and the surrounding liquid  $(\left|Z_{nf}^*\right| \gg \left|Z_{n\ell}^*\right|)$ , we have  $\Delta f_n^* = -\Delta f_{sn}$ .

### 2.1 Special Case - Film Immersed in Liquid

In a liquid medium, the 'membrane' actually corresponds to a bulk, infinitely thick liquid. The impedance ratio is now a ratio of pure material properties:

$$r_{nfm}^* = \left(\frac{\rho_m G_{nm}^*}{\rho_f G_{nf}^*}\right)^{1/2} \tag{16}$$

In the past, we have expressed Eq. 14 in the following way:

$$\frac{\Delta f_n^*}{\Delta f_{sn}} = -\frac{D_{nf}^{*-2} + R_{n\ell}^{*2}}{\cot\left(D_{nf}^*\right)/D_{nf}^* + R_{n\ell}^*}$$
(17)

Here  $R_{n\ell}^*$  defines the ratio of the complex frequency shift for the liquid to the Sauerbrey frequency shift for the film:

$$R_{n\ell}^* = \frac{\Delta f_{n\ell} + i\Delta \Gamma_{n\ell}}{\Delta f_{sn}} \tag{18}$$

## 3 Thin Films

### 3.1 Single Layer

For small  $d/\lambda_n$  we expand the tangent function using  $\tan{(x)} \approx x + x^3/3$  to obtain the following for the dissipation ratio:

$$\frac{-\Delta\Gamma_n}{\Delta f_{ns}} \approx \frac{8\pi^2}{3} \left(\frac{d}{\lambda_n}\right)^2 \tan\left(\frac{\phi_n}{2}\right) = \frac{4\pi^2 f_n^2 M_A^2}{3} \frac{\sin\left(\phi_n\right)}{|G_n^*| \rho}.$$
 (19)

The correction to the Sauerbrey form of  $\Delta f_n$  is very small in this regime, so we can replace  $\Delta f_n$  with  $-\Delta f_{sn}$ , and use Eq. 1 to obtain the following expression for  $\Delta \Gamma_{nt}$ :

$$\Delta\Gamma_{nt} = \frac{8\pi^2 n^3 f_1^4 M_A^3}{3Z_q} \frac{\sin(\phi_n)}{|G_n^*| \rho} = \frac{8\pi^2 n^3 f_1^4 M_A^3 J_n''}{3Z_q \rho}.$$

Here  $J_n''$  is the imaginary component of the complex shear compliance,  $J_n^*$ , with  $J_n^* = 1/G_n^*$ . We can combine equations 14 and 19 to get the following expression for the actual value of  $\Delta\Gamma_n$ , normalized by the form thin film limit:

$$\frac{\Delta\Gamma}{\Delta\Gamma_t} = -\mathrm{imag}\left(\frac{3}{8\pi^2 \tan\left(\phi_n/2\right) \left(d/\lambda_n\right)^2} \frac{\tan\left(D_{nf}^*\right) \left(1 - \left(r_{nfm}^*\right)^2\right)}{D_{nf}^* + i \tan\left(D_{nf}^*\right) r_{nfm}^*}\right) \tag{20}$$

This is what this looks like for different values of the phase angle, and for  $r_{nfm}^* = 0$ .

### 3.2 Two Layers

## 3.2.1 Obtaining J'' from the dissipation

for thin films we can neglect the tangent term in the denominator and replace the leading tangent function with its argument to get:

$$\frac{\Delta f_n^*}{f_{snf}} \approx \left( (r^*)^2 - 1 \right) \tag{21}$$

$$\frac{\Delta f_n^*}{f_{sn}} \approx \left(\frac{Z_{nm,0}}{Z_{nf}^*}\right)^2 - 1 = \frac{(Z_{nm,0})^2}{\rho_f G_f^*} - 1 \tag{22}$$

#### 3.2.2 Perfectly Rigid Membrane

We can use the Sauerbrey form for  $Z_{nm,0}$  (Eq. 4) to get a useful estimate of the response.

$$\frac{\Delta f_n^* + f_{snf}}{f_{snf}} \approx -\left(2\pi n f_1 \rho_m d_m\right)^2 \frac{J_{nf}^*}{\rho_f} \tag{23}$$

Note that the reference point for  $\Delta f_n^*$  is the frequency with just the membrane, which we don't always know as accurately as we would like. When looking at the behavior of very thin films, we will often just  $\Delta\Gamma$  to get  $J_{nf}''$  (we lose the negative sign because  $J^* = J' - iJ''$ :

$$\Delta\Gamma \approx \frac{8\pi^2 n^3 f_1^4}{Z_q} \left(\rho_f d_f\right) \left(\rho_m d_m\right)^2 \frac{J_{nf}''}{\rho_f} \tag{24}$$

$$\frac{\Delta\Gamma}{d_f} \approx \frac{8\pi^2 n^3 f_1^4}{Z_q} (\rho_m d_m)^2 J_{nf}^{"}$$
 (25)

Rearranging for  $J''_{nf}$ , we have:membrane impedance is

$$J_{nf}^{"} = \frac{\rho_f \Delta \Gamma_n}{f_{snf} \left(2\pi n f_1 \rho_m d_m\right)^2} \tag{26}$$

#### 3.2.3 Obtaining $J^*$ or $G^*$

If we do a temperature scan from low temperatures (where the film is glassy and the Sauerbrey expression works for everything), then subtract the low temperature value of  $f_n^*$  from the one at higher temperatures to obtain a quantity we call  $\Delta f_{nT}^*$ , which from Eq. 23 can be written in the following way:

$$\frac{\Delta f_{nT}^*}{f_{snf}} \approx -\left(2\pi n f_1 \rho_m d_m\right)^2 \frac{J_{nf}^*}{\rho_f} \tag{27}$$

The expression for  $G_{nf}^* = 1/J_{nf}^*$  is:

$$G_{nf}^* \approx -\frac{f_{snf}}{\rho_f \Delta f_{nT}^*} \left(2\pi n f_1 \rho_m d_m\right)^2 \tag{28}$$

# 4 Solution Method and Error Analysis

The numerical solution obtains three quantities (typically  $d\rho$ ,  $|G_3\rho|$  and  $\phi$ ) that give predicted three measured quantities in agreement with experimental values. These three measured quantities are two frequency shifts and one dissipation shift. In a  $n_1$ :  $n_2$ ,  $n_3$  calculation, these quantities are  $\Delta f_{n_1}$ ,  $\Delta f_{n_2}$  and  $\Delta \Gamma_{n_3}$ . MATLAB and Python both return the Jacobian, J, at the solution point, which is given by the following expression:

$$J = \begin{bmatrix} \frac{\partial \Delta f_{n_1}}{\partial (d\rho)} & \frac{\partial \Delta f_{n_1}}{\partial (|G_3|\rho)} & \frac{\partial \Delta f_{n_1}}{\partial \phi} \\ \frac{\partial \Delta f_{n_2}}{\partial (d\rho)} & \frac{\partial \Delta f_{n_2}}{\partial (|G_3|\rho)} & \frac{\partial \Delta f_{n_2}}{\partial \phi} \\ \frac{\partial \Delta \Gamma_{n_3}}{\partial (d\rho)} & \frac{\partial \Delta \Gamma_{n_3}}{\partial (|G_3|\rho)} & \frac{\partial \Delta \Gamma_{n_3}}{\partial \phi} \end{bmatrix}$$
(29)

Once we have the matrix, we invert it to get  $J^{-1}$ , the Jacobian of the inverse function, which is what we need:

$$J^{inv} \equiv J^{-1} = \begin{bmatrix} \frac{\partial(d\rho)}{\partial \Delta f_{n_1}} & \frac{\partial(d\rho)}{\partial \Delta f_{n_2}} & \frac{\partial(d\rho)}{\partial \Delta f_{n_2}} & \frac{\partial(d\rho)}{\partial \Delta \Gamma_{n_3}} \\ \frac{\partial(|G_3|\rho)}{\partial \Delta f_{n_1}} & \frac{\partial(|G_3|\rho)}{\partial \Delta f_{n_2}} & \frac{\partial(|G_3|\rho)}{\partial \Delta \Gamma_{n_3}} \\ \frac{\partial\phi}{\partial \Delta f_{n_1}} & \frac{\partial\phi}{\partial \Delta f_{n_2}} & \frac{\partial\phi}{\partial \Delta \Gamma_{n_3}} \end{bmatrix}$$
(30)

The uncertainties in the experimental quantities are  $\Delta f_{n1}^{err}$ ,  $\Delta f_{n2}^{err}$  and  $\Delta \Gamma_{n3}^{err}$ . We represent these as three component error vector:

$$err = \begin{cases} \Delta f_{n1}^{err} \\ \Delta f_{n2}^{err} \\ \Delta \Gamma_{n3}^{err} \end{cases}$$
 (31)

In our linearized analysis we just multiply the uncertainties by the appropriate partial derivatives, and sum the three different uncertainties in quadrature to get the associated experimental uncertainty in our extracted property:

$$(d\rho)^{err} = \left( \left( J_{11}^{inv}err(1) \right)^2 + \left( J_{12}^{inv}err(2) \right)^2 + \left( J_{13}^{inv}err(3) \right)^2 \right)^{0.5}$$

$$(|G_3| \rho)^{err} = \left( \left( J_{21}^{inv}err(1) \right)^2 + \left( J_{22}^{inv}err(2) \right)^2 + \left( J_{23}^{inv}err(3) \right)^2 \right)^{0.5}$$

$$\phi^{err} = \left( \left( J_{31}^{inv}err(1) \right)^2 + \left( J_{32}^{inv}err(2) \right)^2 + \left( J_{33}^{inv}err(3) \right)^2 \right)^{0.5}$$

$$(32)$$

This same analysis can be applied to more complicated models as well.

# 5 Some Other Expressions

We can simplify the area analysis considerably by writing a single function with three equations and three unknowns. For an x:y,z calculation the variables are  $d\rho$ ,  $G\rho_3$  and  $\phi$ . The equations just equate the measured and predicted values of  $\Delta f_x$ ,  $\Delta f_y$  and  $\Delta \Gamma_z$ . Right now many of our expressions are in terms of  $d/\lambda$ , so it's convenient to write this in terms of the variables that we ultimately care about:

$$d/\lambda_n = d\rho f_n \left(\frac{1}{\rho |G_n^*|}\right)^{1/2} \cos(\phi_n/2) \tag{33}$$

The inverse relationship is:

$$\rho |G_n^*| = \left(\frac{d\rho n f_1 \cos(\phi_n/2)}{(d/\lambda_n)}\right)^2 \tag{34}$$

This leads to the following expression for  $D_n^*$ 

$$D_n^* = k_n^* d = \frac{2\pi d\rho f_n}{\left(\rho \left| G_n^* \right| \right)^{1/2}} \left(\cos\left(\phi_n/2\right) - i\sin\left(\phi_n/2\right)\right) = \frac{2\pi f_n d\rho}{Z_n^*}$$
(35)

We'll use the constant phase approximation, so  $\phi$  is assumed to be independent of n. We'll use  $G_3^*$  as our reference, using the following expression for  $|G_n^*|$ :

$$|G_n^*| = |G_3^*| (n/3)^{\phi/90} \tag{36}$$

$$\frac{d}{\lambda_n} = \frac{d}{\lambda_3} \left(\frac{n}{3}\right)^{1-\phi/180} \tag{37}$$

We can also get a relationship between  $\phi$  and  $d\lambda$  at a fixed value of  $J_n''$ , which helps us put the thin film limit in the context of the contour plots for  $r_h$  and  $r_d$ :

$$d/\lambda_n = d\rho n f_1 \left(\frac{|J_n^*|\sin\phi_n}{\rho}\right)^{1/2} \frac{\cos(\phi_n/2)}{\left(\sin\phi_n\right)^{1/2}}$$

### 5.1 Voigt Model

In the power law model commonly employed in our group,  $\phi$  is assumed to be independent of n and the n-dependence of  $d/\lambda_n$  is given by Eq. 37. In the commonly used Voigt model, G' is assumed to be independent of n and G'' is assumed to increase linearly with n:

$$G_n' = G_3' = |G_3^*| \cos \phi_3 \tag{38}$$

$$G_n'' = \frac{n}{3}G_3'' = \frac{n}{3}|G_3^*|\sin\phi_3\tag{39}$$

This model is not rheologically self-consistent, as pointed out by Reviakine *et al.* [21] However, we can use it as a point of comparison to see how much the assumed frequency dependence affects the properties that are extracted from our analysis. Equations 38 and 39 can be combined to give the following expressions for  $|G_n^*|$  and  $\phi_n$ :

$$\phi_n = \arctan\left(\frac{n}{3}\tan\phi_3\right) \tag{40}$$

$$|G_n^*| = |G_3^*| \left(\cos^2(\phi_3) + \frac{n^2}{9}\sin^2(\phi_3)\right)^{1/2}$$
(41)

These expressions can then be used in conjunction with Eq. 33 to get an expression relating  $d/\lambda_n$  to  $d/\lambda_3$  and  $\phi_3$ :

$$\frac{d}{\lambda_n} = \frac{d}{\lambda_3} \frac{n}{3} \left( \cos^2 \left( \phi_3 \right) + \frac{n^2}{9} \sin^2 \left( \phi_3 \right) \right)^{-1/4} \frac{\cos \left( \frac{1}{2} \arctan \left( \frac{n}{3} \tan \phi_3 \right) \right)}{\cos \left( \phi_3 / 2 \right)} \tag{42}$$

# 6 Error determination for $J_3'''$

For thin films, we are most sensitive to  $J_3'' = \sin \phi / |G_3^*|$ . Equivalently, we have:

$$J_3''/\rho = \sin\phi/|G_3^*|\rho \tag{43}$$

or

$$|G_3^*| \rho = \sin \phi / (J_3''/\rho) \tag{44}$$

From the chain rule, we have

$$\frac{\partial \Delta f_{n_1}}{\partial \left( J'' / \rho \right)} = \frac{\partial \Delta f_{n_1}}{\partial \left( \left| G_3^* \right| \rho \right)} \frac{\partial \left( \left| G_3^* \right| \rho \right)}{\partial \left( J'' / \rho \right)} = -\frac{\partial \Delta f_{n_1}}{\partial \left( \left| G_3^* \right| \rho \right)} \frac{\sin \phi}{\left( J_3'' / \rho \right)^2} \tag{45}$$

So to get the Jacobian for for the case where  $|G_3^*| \rho$  is replaced by  $J''/\rho$  we just multiply the middle row in the Jacobian by  $-\sin \phi/(J_3''/\rho)^2$ .

# **Bibliography**

- [1] G. Sauerbrey, Verwendung von Schwingquarzen zur Wägung dünner Schichten und zur Mikrowägung, Zeitschrift für Physik A Hadrons and Nuclei 155 (2) (1959) 206–222. doi:10.1007/BF01337937.
- [2] K. A. Marx, Quartz Crystal Microbalance: A Useful Tool for Studying Thin Polymer Films and Complex Biomolecular Systems at the Solution-Surface Interface, Biomacromolecules 4 (5) (2003) 1099–1120. doi:10.1021/bm020116i.
- [3] M. A. Cooper, V. T. Singleton, A survey of the 2001 to 2005 quartz crystal microbalance biosensor literature: applications of acoustic physics to the analysis of biomolecular interactions, Journal of Molecular Recognition 20 (3) (2007) 154–184. doi:10.1002/jmr.826.
- [4] B. Becker, M. A. Cooper, A survey of the 2006-2009 quartz crystal microbalance biosensor literature, Journal of Molecular Recognition 24 (5) (2011) 754–787. doi:10.1002/jmr.1117.
- [5] A. Tiraferri, P. Maroni, D. Caro Rodríguez, M. Borkovec, Mechanism of Chitosan Adsorption on Silica from Aqueous Solutions, Langmuir 30 (17) (2014) 4980–4988. doi:10.1021/la500680g.
- [6] P. Yi, K. L. Chen, Release Kinetics of Multiwalled Carbon Nanotubes Deposited on Silica Surfaces: Quartz Crystal Microbalance with Dissipation (QCM-D) Measurements and Modeling, Environmental Science & Technology 48 (8) (2014) 4406–4413. doi:10.1021/es405471u.
- [7] J. Song, W. E. Krause, O. J. Rojas, Adsorption of polyalkyl glycol ethers and triblock nonionic polymers on PET, Journal of Colloid and Interface Science 420 (2014) 174–181. doi:10.1016/j.jcis.2014.01.012.
- [8] I. E. Salama, B. P. Binks, P. D. Fletcher, D. I. Horsup, Adsorption of benzyldimethyldodecylammonium chloride onto stainless steel using the quartz crystal microbalance and the depletion methods: an optimisation study, Colloids and Surfaces A: Physicochemical and Engineering Aspects 447 (2014) 155–165. doi:10.1016/j.colsurfa.2014.01.034.
- [9] A. Rudrake, K. Karan, J. H. Horton, A combined QCM and XPS investigation of asphaltene adsorption on metal surfaces, Journal of colloid and interface science 332 (1) (2009) 22–31.
- [10] Z. Liu, H. Choi, P. Gatenholm, A. R. Esker, Quartz Crystal Microbalance with Dissipation Monitoring and Surface Plasmon Resonance Studies of Carboxymethyl Cellulose Adsorption onto Regenerated Cellulose Surfaces, Langmuir 27 (14) (2011) 8718–8728. doi:10.1021/la200628a.

- [11] J. Wegener, A. Janshoff, C. Steinem, The quartz crystal microbalance as a novel means to study cell-substrate interactions in situ, Cell Biochemistry and Biophysics 34 (1) (2001) 121–151.
- [12] D. A. Buttry, M. D. Ward, Measurement of Interfacial Processes at Electrode Surfaces with the Electrochemical Quartz Crystal Microbalance, Chem. Rev. 92 (1992) 1355–1379.
- [13] A. Hillman, The Electrochemical Quartz Crystal Microbalance, in: A. J. Bard, M. Stratmann, P. R. Unwin (Eds.), Encyclopedia of Electrochemistry, Volume 3, Instrumentation and Electroanalytical Chemistry, Vol. 3, Wiley-VCH, Weinheim, 2003, pp. 230–289.
- [14] D. Johannsmann, Viscoelastic, mechanical, and dielectric measurements on complex samples with the quartz crystal microbalance, Physical Chemistry Chemical Physics 10 (31) (2008) 4516–4534.
- [15] G. C. DeNolf, L. Haack, J. Holubka, A. Straccia, K. Blohowiak, C. Broadbent, K. R. Shull, High Frequency Rheometry of Viscoelastic Coatings with the Quartz Crystal Microbalance, Langmuir 27 (16) (2011) 9873–9879. doi:10.1021/la200646h.
- [16] M. V. Voinova, M. Rodahl, M. Jonson, B. Kasemo, Viscoelastic Acoustic Response of Layered Polymer Films at Fluid-Solid Interfaces: Continuum Mechanics Approach, Physica Scripta 59 (5) (1999) 391–396. doi:10.1238/Physica.Regular.059a00391.
- [17] F. Simonetti, P. Cawley, On the nature of shear horizontal wave propagation in elastic plates coated with viscoelastic materials, Proceedings of the Royal Society A: Mathematical, Physical and Engineering Sciences 460 (2048) (2004) 2197–2221. doi:10.1098/rspa.2004.1284.
- [18] D. Johannsmann, Viscoelastic analysis of organic thin films on quartz resonators, Macromol. Chem. Phys. 200 (1999) 501–516.
- [19] D. A. Brass, K. R. Shull, Contact Studies of Weakly Compressed PEG Brushes with a Quartz Crystal Resonator, Langmuir 22 (2006) 9225–9233. doi:10.1021/la061793r.
- [20] D. A. Brass, K. R. Shull, Membrane-enhanced surface acoustic wave analysis of grafted polymer brushes, Journal of Applied Physics 103 (7) (2008) 073517. doi:10.1063/1.2903880.
- [21] I. Reviakine, D. Johannsmann, R. P. Richter, Hearing What You Cannot See and Visualizing What You Hear: Interpreting Quartz Crystal Microbalance Data from Solvated Interfaces, Analytical Chemistry 83 (23) (2011) 8838–8848. doi:10.1021/ac201778h.